Mechanism of Dioxygen Cleavage in Tetrahydrobiopterin-Dependent Amino Acid Hydroxylases

Arianna Bassan,* Margareta R. A. Blomberg, and Per E. M. Siegbahn[a]

Abstract: The reaction mechanism for the formation of the hydroxylating intermediate in aromatic amino acid hydroxylases (i.e., phenylalanine hydroxylase, tyrosine hydroxylase, tryptophan hydroxylase) was investigated by means of hybrid density functional theory. These enzymes use molecular oxygen to hydroxylate both the tetrahydrobiopterin cofactor and the aromatic amino acid. A mechanism is proposed in which dioxygen forms a bridging bond between the cofactor and iron. The product is an iron(II)–peroxy–pterin intermediate, and iron was found to be essential for the catalysis of this step. No stable intermediates involving a pterin radical cation and a superoxide ion O_2^- were found on the reaction pathway. Heterolysis of the O–O bond in the iron(II)–peroxy–pterin intermediate is promoted by one of the water molecules coordinated to iron and releases hydroxypterin and the high-valent iron oxo species Fe^{IV}=O, which can carry out subsequent hydroxylation of aromatic rings. In the proposed mechanism, the formation of the bridging C–O bond is rate-limiting in the formation of Fe^{IV}=O.

Keywords: density functional calculations · enzyme catalysis · O–O activation · hydroxylation · reaction mechanisms

Introduction

Tetrahydrobiopterin-dependent hydroxylases form a family of non-heme oxygen-activating iron enzymes that catalyze hydroxylation of aromatic amino acids.[1–3] Tetrahydrobiopterin is an essential cofactor for these metalloproteins, which comprise phenylalanine hydroxylase (PAH), tyrosine hydroxylase (TyrH), and tryptophan hydroxylase (TrpH). The functions of these enzymes are shown in Scheme 1.

Phenylalanine hydroxylase, which is mainly located in the liver and to a less extent in the kidneys, is involved in the rate-limiting step of phenylalanine catabolism, which passes through the degradation of phenylalanine to tyrosine.[1] Deficiency of phenylalanine hydroxylase in the body leads to phenylketonuria, an inborn error of the metabolism that causes severe mental retardation.[2] Hydroxylases TyrH and TrpH are associated with the vital biosynthesis of neurotransmitters and hormones. In the nervous system TyrH converts tyrosine to L-Dopa, from which the catecholamines dopamine, adrenaline, and noradrenaline are derived. In the central nervous system TrpH participates in the rate-limiting step of serotonin synthesis, which starts with the transformation of tryptophan to 5-hydroxytryptophan. Malfunction of TyrH is believed to correlate to psychological disorders such as manic-depressive illness, schizophrenia, and Gilles de la Tourette's syndrome.[1] Parkinson's disease has also been associated with TyrH function. Physiological processes related to the neurotransmitter serotonin, which is also a precursor of melatonin, such as the circadian rhythm, are probably affected by the enzymatic activity of TrpH.[1]

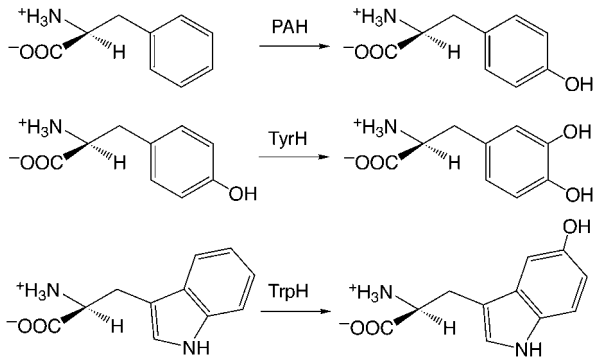

Scheme 1. Hydroxylation of aromatic amino acids catalyzed by phenylalanine hydroxylase (PAH), tyrosine hydroxylase (TyrH) and tryptophan hydroxylase (TrpH).

Besides sharing a common task, namely, hydroxylation of an aromatic ring, pterin-dependent hydroxylases have pronounced mechanistic and structural similarities. The catalytic cores of these homotetrameric enzymes contain an Fe^{II} ion coordinated by the so-called 2-His-1-carboxylate facial tri-

[a] A. Bassan, Prof. M. R. A. Blomberg, Prof. P. E. M. Siegbahn
Department of Physics
Stockholm Center for Physics, Astronomy and Biotechnology
Stockholm University
10691, Stockholm (Sweden)
Fax: (+46) 8-55378600
E-mail: arianna@physto.se

0947-6539/03/0901-0106 $ 20.00+.50/0

ad.[4, 5] The aromatic amino acids also all undergo hydroxylation by molecular oxygen coupled with two-electron oxidation of the cofactor (6*R*)-L-erythro-5,6,7,8-tetrahydrobiopterin (BH_4) to 4a-(*S*)-hydroxydihydrobiopterin, also known as pterin 4a-carbinolamine (Scheme 2). Subsequently, this species evolves to the dehydrated quinoid dihydropterin, and BH_4 is then regenerated by dihydropteridine reductase.[2]

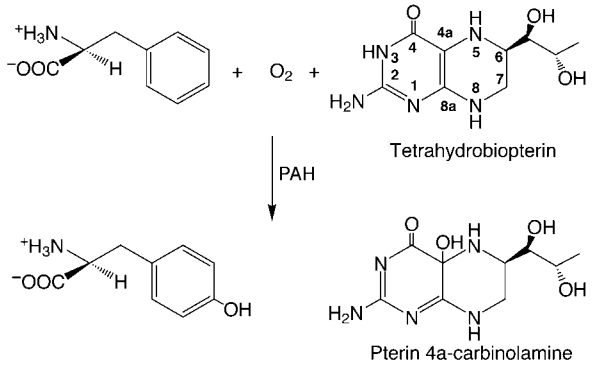

Scheme 2. Hydroxylation of the cofactor and of the aromatic amino acid catalyzed by phenylalanine hydroxylase (PAH).

Due to the sequential and structural homology and the resemblance of the chemical transformations occurring in PAH, TyrH, and TrpH, it is a common belief that these three enzymes have similar hydroxylation mechanisms.[3] Significant progress in the understanding of the activity of the aromatic amino acid hydroxylases has been acquired mainly from investigations on PAH because of its stability, but studies on TyrH have also given important information. Mechanistic studies show that both the Fe^{II} center and the organic cofactor are required for aromatic hydroxylation to occur. However, the exact roles of iron and BH_4 in the reaction mechanism is still unclear, with different opinions regarding the activity of the metal in the formation of the hydroxylating intermediate.

Kinetic studies on TyrH revealed, rather surprisingly, large ^{18}O isotope effects,[6, 7] but no solvent[8] or primary isotope effect.[9] These observations were interpreted to show a change in bond order but no cleavage of dioxygen in the rate-determining step of the enzymatic catalysis.[7, 10] The magnitude of the isotope effects also led to the conclusion that the rate-determining step is unlikely to involve formation of an iron–oxygen bond. Experiments with alternative or isotopically labeled substrates suggested that amino acid hydroxylation is not rate-limiting for PAH and TyrH.[8, 11] Therefore, at least for these two hydroxylases, the formation of the hydroxylating intermediate is proposed to be rate-limiting in catalysis.[12] A recent mechanistic investigation on TrpH[13] showed that the turnover numbers for PAH and TyrH are substantially higher than that of TrpH. This observation has been connected to the specific substrate leading to a slower hydroxylation step in the case of TrpH, rather than to slow formation of the hydroxylating intermediate.

The identity of the hydroxylating intermediate therefore becomes crucial for understanding the catalytic activity of pterin-dependent hydroxylases. Direct involvement of the cofactor in the formation of this key intermediate fits the experimental observation that molecular oxygen is the source of the oxygen in the oxidized hydroxypterin in PAH.[14] A peroxy intermediate is therefore likely to be formed during the catalytic cycle. The other oxygen atom of O_2 is incorporated into the hydroxylated aromatic amino acid.[11]

Steady-state kinetic experiments on TyrH[9] indicated a sequential mechanism in which pterin binds first, then dioxygen and the substrate. For PAH allosteric activation of phenylalanine in the regulatory domain requires phenylalanine to bind first, but in the preactivated enzyme a more random order of substrate binding is observed.[1] Despite the specific binding order, all three substrates must be bound before any product is released by pterin hydroxylases.

The similarities of the functional properties of the pterin enzymes with those of P450-dependent enzymes,[15] which are also capable of hydroxylating unactivated aromatic C–H substrates, suggest that the iron atom probably plays a fundamental role in dioxygen activation. In the generally accepted mechanism for P450, a high-valent ferryl oxo species is formed after O–O cleavage of an iron peroxy intermediate. A mechanism involving a ferryl intermediate was therefore also proposed for the pterin-dependent hydroxylases, as shown in Scheme 3.[10, 16, 17]

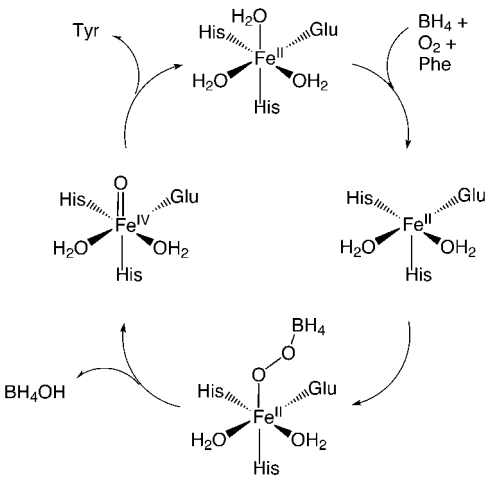

Scheme 3. Mechanism proposed for the formation of the hydroxylating intermediate in aromatic amino acid hydroxylases.[17]

In this mechanism dioxygen is activated by the metal center by formation of an iron–peroxy–pterin intermediate. The specific role played by iron in dioxygen activation is not yet clear. In fact, the question whether O_2 binds in the first coordination shell of the iron(II) complex or not is still controversial, because an $Fe-O_2$ complex has not been directly observed. Heterolytic O–O cleavage in the iron peroxy intermediate leads to two products: the high-valent iron oxo hydroxylating intermediate Fe^{IV}=O and the hydroxylated cofactor. The hydroxylation of the amino acid by Fe^{IV}=O concludes the chemical transformations performed in these enzymes. This mechanism is supported by experiments on model systems, which showed that a non-heme Fe^{IV}=O species is capable of arene hydroxylation.[18]

The crystal structures of phenylalanine hydroxylase[19] and tyrosine hydroxylase[20] with pterin bound in the oxidized

  0947-6539/03/0901-0107 $ 20.00+.50/0

form (7,8-dihydro-L-biopterin, BH_2) support the possibility that an iron–peroxy–pterin intermediate is formed. In these structures the metal center is in the inactive Fe^{III} form, which is the usual oxidation state of the metal when the enzyme is isolated and which is prereduced by BH_4 to Fe^{II} before enzymatic catalysis starts.[3] A recent high-resolution X-ray analysis of the Fe^{II} form of the binary complex PAH–BH_4 detected very small structural changes with respect to the Fe^{III} form PAH–BH_2.[21]

In the crystal structures the cofactor is located in the second coordination shell of the iron center, π stacking with a phenyl ring (Phe254 in PAH and Phe300 in TyrH). Figure 1 illustrates the detailed interactions of pterin at the catalytic site, as

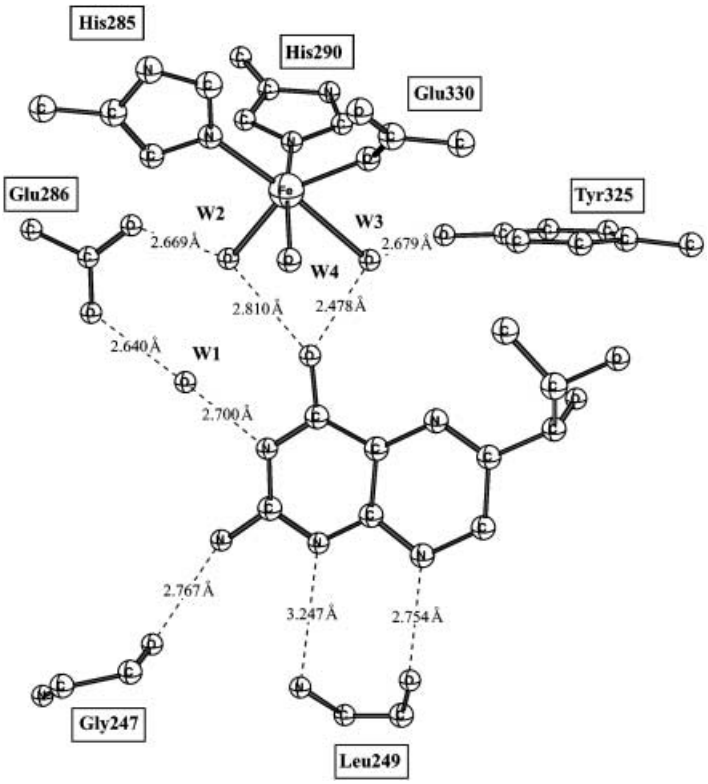

Figure 1. X-ray crystal structure of the catalytic site of PAH.[19]

determined in the structure of a binary complex of PAH with BH_2 at 2.0 Å resolution.[19] A 2-His-1-carboxylate ligation is provided by Glu330, His285, and His290, and the octahedral coordination sphere of iron is completed by three water molecules (W2, W3, W4). The same type of coordination is also found for PAH without bound pterin.[19] In proximity to the metal center, tyrosine residue Tyr325 forms a hydrogen bond with W3. Although this tyrosine residue is highly conserved in the pterin hydroxylases, its direct involvement in the catalytic cycle seems to be excluded.[19] The distance between the iron atom and C4a of pterin is 6.1 Å, while the carbonyl oxygen atom of pterin is located within hydrogen-bonding distance of the two water ligands W2 and W3. Water molecule W2 forms a hydrogen bond with Glu286, which in turn interacts with N3 of pterin via a mediating water molecule (W1). Glu286 is essential for a correct functioning of PAH.[22] A series of hydrogen-bonding interactions between pterin and other residues were identified in the crystal structure (Figure 1, where the roles of Leu249 and Gly247 are highlighted). Mutations of these residues seem to occur in patients affected by phenylketonuria.[23] A similar structural arrangement of the active site is found in the crystal structure solved for TyrH at a resolution of 2.2 Å, in which only two water ligands were detected, that is, a five-coordinate iron center.[20] A slightly different structural arrangement was assigned on the basis of ^1H NMR studies[24] on the enzyme-bound Phe and BH_2 with iron still in the Fe^{III} form. The iron atom and C4a of the cofactor are somewhat closer (4.3 Å), and the deduced distance between the iron atom and the carbonyl oxygen atom of pterin seems to place the cofactor in the first coordination sphere of the metal center.

The catalytically active Fe^{II} form of the enzyme was studied by CD and MCD spectroscopy,[25, 26] which provided a detailed picture of the electronic structure of the high-spin Fe^{II} center and which supports the coupled mechanism presented in Scheme 3.[17] The sixfold coordination of the metal atom is maintained in Phe-bound Fe^{II}-PAH and in BH_4-bound Fe^{II}-PAH, although a slight perturbation of the geometry at the metal center is observed with the bound amino acid substrate. When both the cofactor and the substrate are bound to Fe^{II}-PAH, substantial perturbations are observed in the ligand field that indicate a change toward fivefold coordination of the metal atom, which then has one free coordination site for oxygen activation.

Here, density functional theory (DFT) is employed to elucidate the role played by the iron site and the cofactor in the mechanism of pterin hydroxylases. The details of the chemical transformations leading to the iron oxo hydroxylating intermediate, as proposed in Scheme 3, were thus examined for a model derived from the crystal structure of BH_2-bound PAH.[19] The steps involving the formation of the iron–peroxy–pterin intermediate and the subsequent O–O bond cleavage to give oxidized hydroxypterin and the iron oxo intermediate are probed.

Methods of Calculation

The reaction mechanism leading to the hydroxylating intermediate in aromatic amino acid hydroxylases was investigated by DFT methods with the B3LYP functional,[27] which includes the Becke three-parameter exchange[28] and the Lee, Yang, and Parr correlation.[29]

Jaguar 4.1[30] was used for geometry optimizations and to explore the potential energy surfaces. Gaussian 98[31] served to compute molecular Hessians (second derivatives of the energy with respect to the nuclear coordinates), through which zero-point corrections and entropy effects could be evaluated. Since an explicit Hessian is needed in the saddle-point optimizations, the geometries of the transition states were also determined with Gaussian 98. An effective core potential[32] was used to describe the iron atom. In the geometry optimizations all the other atoms were described by a standard double-zeta basis set, labeled lacvp in Jaguar and lanl2dz in Gaussian. The lanl2dz basis set was also used to calculate the molecular Hessians. By optimizing one minimum with the lanl2dz and the lacvp basis sets, it was checked that the two different basis sets give similar structures and similar relative energies. The resulting energy difference, calculated with one of the double-zeta basis sets for the two differently optimized structures is about 0.5 kcal mol^{-1}.

The final B3LYP energies for the fully optimized structures were evaluated by using a large basis set with polarization functions on all atoms (labeled

0947-6539/03/0901-0108 $ 20.00+.50/0 *Chem. Eur. J.* **2003**, *9*, No. 1

lacv3p** in Jaguar).[30] The energies reported here are free energies including zero-point and thermal effects. Thermal effects were evaluated for a temperature of 298.15 K.

By modeling the solvent as a macroscopic continuum with dielectric constant ε and the solute contained in a cavity of this continuous medium, long-range solvent effects could be included in the calculation. Specifically, the self-consistent reaction field method, as implemented in Jaguar[33, 34] was used to evaluate the solvent corrections by employing the lacvp basis set. A low dielectric constant ($\varepsilon = 4$) was chosen to model the protein environment together with a probe radius of $R = 1.40$ Å corresponding to the water molecule. In general, the description of the solvent as a continuum is sufficiently accurate to take into account the rather small effects of the protein environment.[35, 36] However, an important exception to this occurs for the binding of dioxygen to the metal complex[37] (see below).

The performance of the B3LYP method has been investigated by using the G2 benchmark tests[38, 39] on a reference set of molecular properties for small compounds of first- and second-row elements, which showed that hybrid DFT methods perform almost as well as the G2 method. The B3LYP method becomes somewhat less accurate when transition metals are involved[36] or when transition states are computed. An overall average error of 3–5 kcal mol^{-1} is expected for the calculated relative energies presented here.

Results and Discussion

The formation of the hydroxylating intermediate in pterin-dependent hydroxylases addressed here mainly follows the mechanism proposed in Scheme 3. In this scheme the iron center plays a crucial role in oxygen activation by driving the chemical reaction toward an iron–peroxy–pterin intermediate. Subsequent O–O cleavage of this species leads to the high-valent iron oxo intermediate Fe^{IV}=O, which should be capable of hydroxylating aromatic rings.[18] The actual reaction mechanism of Fe^{IV}=O with aromatic amino acids has not yet been probed. The following three subsections describe in detail the proposed chemical transformations by which the Fe^{IV}=O hydroxylating intermediate is generated. The first subsection deals with the reactants, the second with the formation of the iron peroxy intermediate, and the third with O–O cleavage to give 4a-carbinolamine (hydroxylated pterin) and the high-valent iron oxo intermediate.

The model employed to investigate the chemical transformations at the active site of aromatic amino acid hydroxylases was based on the crystal structure of phenylalanine hydroxylase in its binary complex with the cofactor,[19] as shown in Figure 1. In the model the 2-His-1-carboxylate facial triad of the iron complex is reduced to two imidazoles and a formate ion. The cofactor is placed in the second coordination shell of the iron complex and forms hydrogen bonds to two water molecules coordinated to the metal atom. Glu286, represented by a formate ion, is also included in the model, together with the water molecule W1, which forms a hydrogen bond to N3 of the cofactor. Residue Glu286 was included due to the experimental observation that it might play a critical role during catalysis.[19, 22] Furthermore, Glu286 and the bridging water molecule are intended to partially take into account the strain imposed by the enzyme on the cofactor, which is otherwise anchored only through the two water molecules of the iron coordination shell.

Non-heme iron-bound dioxygen: CD/MCD spectroscopic studies on PAH showed that, when both phenylalanine and BH_4 simultaneously bind at the active site, a structural change occurs, interpreted as a water molecule leaving the octahedral coordination shell of the metal center, where ultimately dioxygen might enter. The optimized five-coordinate structure in which the vacancy has been created *trans* to His290 is shown in Figure 2. Experimental observations indicate that

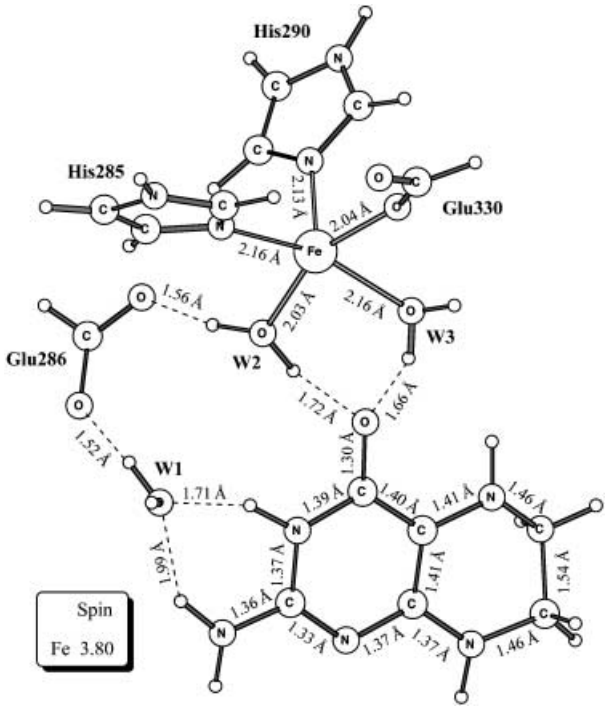

Figure 2. Optimized structure and spin distribution for the quintet ground state of the pentacoordinate iron complex with the cofactor in the second coordination shell.

two of the water molecules are loosely bound to iron (W3, W4 in Figure 1), but it is not known which of these two water molecules might leave the iron coordination shell.[21] In the present study W4 was chosen, since this leads to the most suitable structure for probing the formation of an iron–peroxy–pterin intermediate. Since a water molecule leaves the iron coordination shell it might be expected that its binding energy to the iron complex would be small. However, the computed binding energy of the water molecule in the six-coordinate iron complex is actually quite high (22.5 kcal mol^{-1}). This value does not include any entropy effect, but even if this were large it could not possibly favor the complete removal of W4 without a strong compensating effect. The mechanism of water removal therefore involves a very strong hydrogen bond between W4 and Glu330, which favors an almost zero-cost conformational change at the iron center by placing W4 in the second coordination shell of iron, which in turn becomes five-coordinate. The calculated energy difference between the 5(+1)- and six-coordinate structures is only 3.2 kcal mol^{-1}. This result agrees with recent X-ray crystallographic data, which suggested that the conformation of Glu330 might play an important role in oxygen activa-

tion.[21] Since W4 is in the second coordination shell during the formation of the hydroxylating intermediate, it is not believed to play any role in the reaction and it was therefore removed from the model (see Figure 2). The total charge of this model is zero, having an Fe^{II} center and two negatively charged formate groups. The optimized pentacoordinate metal complex adopts a square-pyramidal structure, which is in agreement with the structure proposed on the basis of the CD/MCD spectroscopic data. The field created by the 2-His-1-carboxylate facial triad is weak, and the result is a high-spin quintet ground state with a spin of 3.80 on Fe^{II}, which is fairly typical. The distance of 6.18 Å between the metal ion and the C4a site of pterin is comparable to the corresponding distance determined by X-ray crystallography (5.9–6.1[19, 21]).

In analogy with many heme-containing oxygenases which pass through an Fe^{II} dioxygen complex, a vacancy is thus created where oxygen can be accommodated and activated. The following section shows that an iron–peroxy–pterin intermediate can be readily formed when dioxygen is allowed to bind directly to the metal atom. In fact, this is a necessary condition for dioxygen to be reduced by the cofactor. Calculating an accurate binding energy for dioxygen to the five-coordinate metal center is a very difficult task, which was recently shown to require the use of QM/MM models.[37] A QM/MM study on dioxygen binding to hemerythrin, a non-heme iron protein, showed that the resulting free energy is significantly affected by van der Waals and electrostatic contributions from the protein environment. For O_2 binding to hemerythrin, a correction of about -10 kcal mol^{-1} originating from the protein environment almost canceled the pronounced entropy effects due to the trapping of molecular oxygen by the metal complex. In the present study the binding of dioxygen to the metal center of pterin-dependent hydroxylases was computed to be endergonic by 10.3 kcal mol^{-1} (solvent effects not included) for the model in Figure 2. Here it is simply assumed that the van der Waals and electrostatic effects of the protein would essentially cancel this energy, as they do for hemerythrin, and lead to a binding of dioxygen which is either exergonic or thermoneutral, or at least not strongly endergonic. Proof of this will require future QM/MM studies.

The geometrical arrangements of the metal ligands and the cofactor are not significantly affected by O_2 binding. However, the paramagnetic molecular oxygen changes the total multiplicity of the iron complex, whose electronic ground state becomes a septet ($M=7$), as shown in Figure 3. This electronic distribution is explained by considering that the iron dioxygen complex is formally written as either $Fe^{2+}O_2$ or $Fe^{3+}O_2^-$, or a resonance hybrid of these two forms. The actual electronic structure involves partial electron transfer from iron to oxygen. The spin on iron is 4.07 and the total spin on dioxygen is 1.53. The superoxide formula $Fe^{3+}O_2^-$ gives a better representation of the quintet state of the iron dioxygen complex, which lies 5.1 kcal mol^{-1} above the septet ground state. As indicated in Table 1, which compares the two spin states, the quintet iron dioxygen complex is characterized by almost one unpaired electron located on dioxygen, with spins of 0.20 and 0.54 on O1 and O2, respectively. This unpaired electron density is antiferromagnetically coupled to the five d electrons of the Fe^{III} ion. The spin on iron of 4.21 shows that the spin is somewhat delocalized on the ligands, as usual. The geometrical details of the two different spin states are quite similar, and both include a hydrogen-bonding interaction between dioxygen and one of the water ligands (W3).

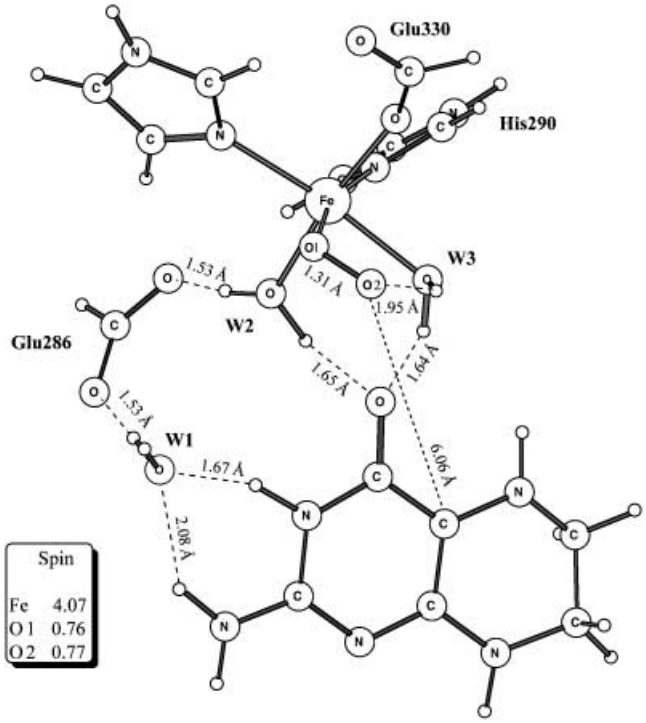

Figure 3. Optimized structure and spin distribution of the ground state ($M=7$) of the iron dioxygen complex.

The iron–peroxy–pterin complex: Following the mechanism in Scheme 3, the next step should be formation of the bridging iron–peroxy–pterin intermediate. The calculations show that when dioxygen is reduced to peroxide two electrons are supplied by the pterin cofactor, which thus becomes positively charged, and iron goes back to its initial Fe^{II} oxidation state. With iron in the Fe^{II} state, one positive charge on the cofactor, one negative charge on Glu286, and two negatively charged formate ligands, the peroxide species, and Glu330, the neutrality of the model complex is maintained. The weak ligand field created by these types of ligands leads to a quintet ground state for this complex. The potential energy surfaces were explored for the quintet, triplet, and septet spin states, and it was found that the reaction path lowest in energy involves the quintet state. The triplet state, corresponding to a

Table 1. Comparison of geometrical parameters [Å] and spin distributions of the septet and quintet states of the iron(II) dioxygen complex.

	d(Fe–O1)	d(O1–O2)	d(O2–W3)	d(Fe–C4a)	Spin(Fe)	Spin(O1)	Spin(O2)
septet ($M=7$)	2.24	1.31	1.95	6.06	4.07	0.76	0.77
quintet ($M=5$)	2.09	1.36	1.77	5.86	4.21	−0.20	−0.54

0947-6539/03/0901-0110 $ 20.00+.50/0 *Chem. Eur. J.* **2003**, *9*, No. 1

low-spin coupling of the unpaired electrons on iron, leads to an iron–peroxy–pterin intermediate substantially higher in energy than the quintet state. A septet state for the iron–peroxy–pterin intermediate was also investigated. This state corresponds to Fe^{III} and a radical on the cofactor, which now becomes neutral. The septet state was found to have no minimum for a bridging peroxide structure, and it decays to the original reactants with dioxygen coordinated to iron. This result, together with the spin distribution obtained for the quintet state of the iron–peroxy–pterin intermediate (see below), means that involvement in the reaction pathway of an Fe^{III}–OOR species, which was proposed as a possible intermediate in the pterin-dependent hydroxylases,[40] is unlikely.

Hence, the reactant iron dioxygen complex, which has a septet ground state, first must be excited to its quintet state, which only costs 5.1 kcal mol^{-1}. This first step is thus spin-forbidden, but should still be quite fast due to the large spin-orbit coupling of iron. Once on the quintet potential surface, the bound dioxygen is ready to carry out the required oxidation reactions.

As the cofactor approaches the metal center, the iron–peroxy–pterin complex can be generated by attack of activated O_2 on the C4a site of the cofactor. This involves electron flow from pterin toward dioxygen, and a charge separation is established due to the electron deficiency created on the pterin ring. According to the resonance forms which can be drawn for the peroxy–pterin intermediate, the positive charge is mainly distributed on the pyrimidine ring between N2 and N3, as shown in Figure 4, which also shows the transition state for dioxygen reduction. This is the transition state for the formation of the new C4a–O bond. A stable cationic radical intermediate in which electron transfer from pterin to dioxygen had occurred prior to the C4a–O bond formation could not be located.

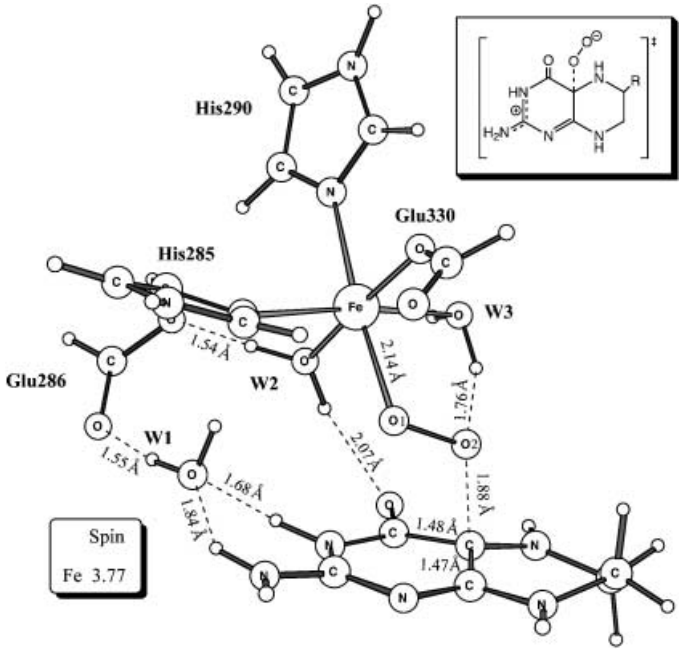

Figure 4. Optimized structure and spin distribution for the quintet transition state leading to the formation of an iron–peroxy–pterin intermediate. The charge separation, which follows the oxidative reaction of the cofactor, is highlighted.

Compared to the quintet form of the metal dioxygen complex, which was described above as an Fe^{III} superoxide, the iron in the transition state for C4a–O bond formation is in the initial Fe^{II} oxidation state, as suggested by the spin of 3.77 on the metal atom. The zero spin population on both pterin and dioxygen indicates that the electron transfer and the related carbon–oxygen bond formation are almost complete at the transition state. This also follows from the bond lengths of the pterin rings, which indicate that the electronic structure has changed to that of the product. For example, the C4a–C8a double bond in the reactant has changed to a single bond, as in the peroxy-pterin intermediate. Since iron has oxidation state II in the reactant (i.e., the septet form of the iron dioxygen complex) and in the iron–peroxy–pterin intermediate, it could be argued that iron seems to be only a spectator during the oxidation of the cofactor with dioxygen. However, iron is essential for the oxidation reaction to occur. Calculations show that a similar mechanism is impossible without the presence of the metal atom. After activating dioxygen in the quintet iron dioxygen complex, iron plays a crucial role in stabilizing the negative charge developing on dioxygen. As shown by the crystal structure, the hydrophobic pocket in which the metal complex is situated and the cofactor binds does not have any positively charged residue which could perform an analogous task.[19] Interestingly, flavin, a cofactor which strongly resembles pterin, can be oxidized by dioxygen in glucose oxidase (GO).[41] However, in this case a charged histidine residue is available to stabilize the negative charge developing on dioxygen.[42] In the aromatic amino acid hydroxylases another role of iron is to catalyze the spin-forbidden part of the reaction between pterin and the paramagnetic dioxygen.

The calculated activation energy for the chemical transformation leading to the iron–peroxy–pterin complex from the septet ground state of the bound dioxygen iron complex is 16.6 kcal mol^{-1}. As shown in Figure 5, which presents the energetics for the entire reaction mechanism, 16.6 kcal mol^{-1} is also the rate-limiting barrier for formation of the hydroxylating intermediate Fe^{IV}=O, since the following transition state for O–O cleavage lies at a lower energy. Transition-state theory allows the calculated energetics to be compared with the experimental V_{max} value measured for PAH isolated from rat liver, which gives an experimental barrier of 15.6 kcal mol^{-1} ($V_{max} = 22$ s^{-1} subunit^{-1}[43]). Since in PAH the slow step in catalysis is the formation of the hydroxylating intermediate,[12] this experimental value can be directly compared to that of 16.6 kcal mol^{-1} calculated here. The calculated result also confirms the experimental observation that a change in bond order of dioxygen should occur during the rate-determining step of the reaction, as shown by the isotope effects found when labeled O_2 was used in kinetic experiments with tyrosine hydroxylase.[7] In these experiments an average value of 1.0175 was measured. An attempt was here made to estimate the oxygen-isotope effect by computing the $k/^{18}k$ ratio, where k and ^{18}k are rate constants derived on the basis of transition-state theory for O_2 and $^{18}O_2$, respectively. The calculated ratio of 1.0363 can be expressed

  0947-6539/03/0901-0111 $ 20.00+.50/0

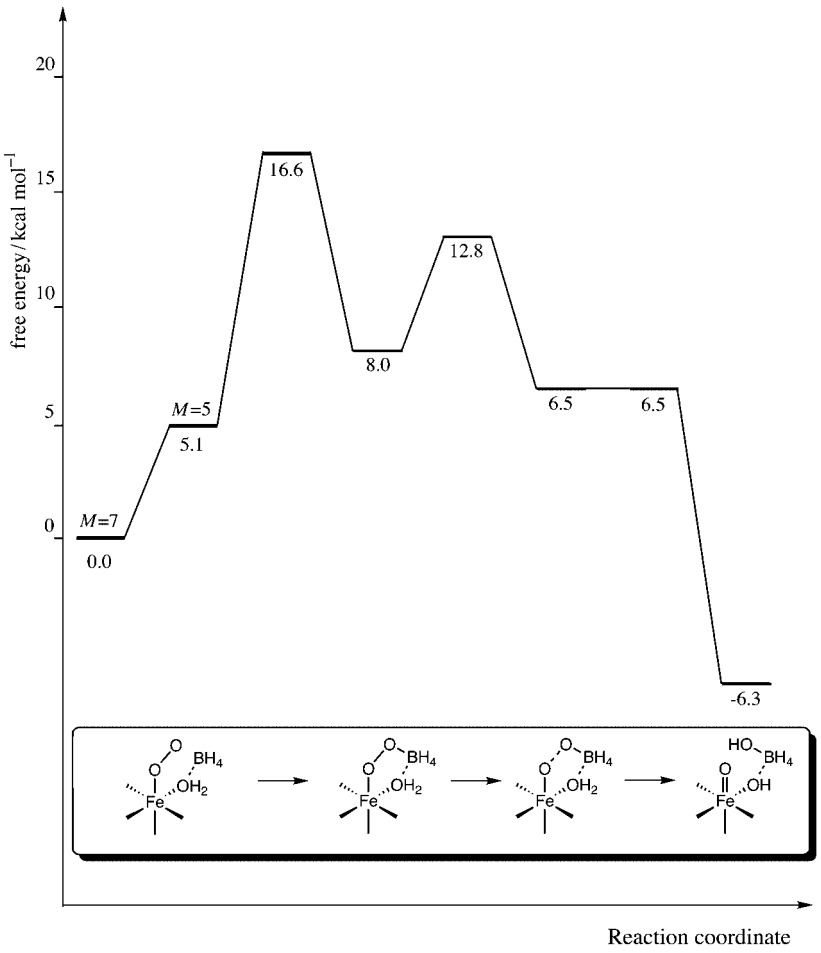

Figure 5. Energy diagram for the suggested reaction mechanism for the formation of the hydroxylating intermediate Fe^{IV}=O in aromatic amino acid hydroxylases.

as a product of zero-point (0.9697) and thermal effects (1.0687). Interestingly, an inverse isotope effect results if only the zero-point effects are considered.

The transition state in Figure 4 leads to the iron–peroxy–pterin intermediate shown in Figure 6, which lies 8.0 kcal mol^{-1} higher in energy than the septet ground state of the iron dioxygen complex (see Figure 5). In this intermediate iron is still in the Fe^{II} state, as indicated by its spin population of 3.78, with some minor spin density on the ligands. One of these ligands is the peroxy–pterin species, for which the calculated O–O bond length is 1.58 Å and hybridization of C4a of pterin has changed from sp^2 to sp^3. For the further development of the reaction, the hydrogen bond between one of the two water molecules coordinated to iron (W3) and the oxygen atom bound to C4a of pterin (O2) is also important. The water ligand is in fact prepared to become a proton source for the following formation of the hydroxylated cofactor 4a-carbinolamine.

In the charge separation established during the oxidation process of the cofactor, a positive charge is delocalized in the pyrimidine ring. Pterin could in principle become neutral by transferring one proton from N2 or N3 to the carboxylate group of Glu286 via a mediating water molecule (W1). Investigation of this possible proton transfer indicated that the protonated peroxy-pterin species is slightly favored over the neutral pyrimidine ring. Therefore, heterolysis of the O–O bond was investigated for the protonated iron–peroxy–pterin intermediate.

Note that although Glu286 does not play any significant role in the reaction mechanism, its presence in the model is essential for investigating the reaction step in which the new C4a–O bond is formed. Glu286 is not involved directly in the oxidation reaction, but rather orients and structurally guides the cofactor during the formation of the peroxide species. A comparison between the X-ray structure and the optimized structure of the peroxide intermediate shows that no significant changes occur in the first coordination shell of the metal atom when the new C4a–O bond is formed, but redirection of the cofactor with respect to the orientation found in the crystal structure is needed for the peroxy–pterin intermediate to be generated.

O–O cleavage: Heterolytic cleavage of the O–O bond in the iron–peroxy–pterin inter-

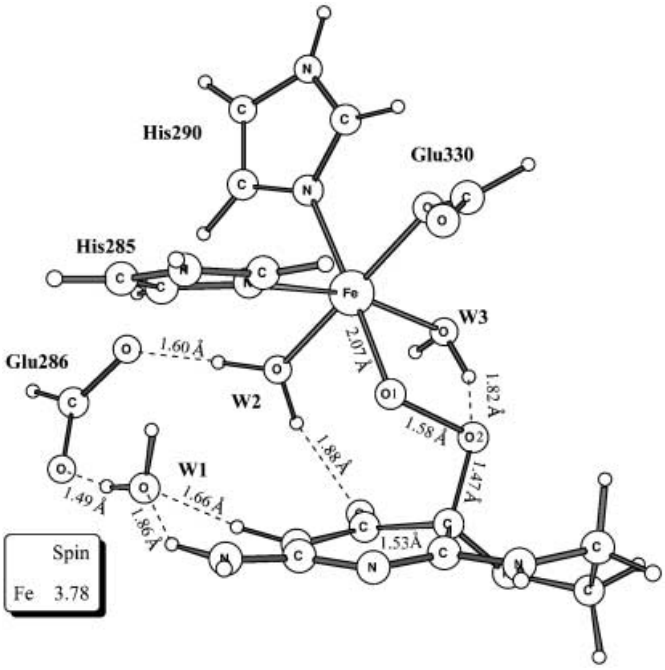

Figure 6. Optimized structure and spin distribution of the iron–peroxy–pterin intermediate, in which the new C4a–O bond has been formed.

0947-6539/03/0901-0112 $ 20.00+.50/0 *Chem. Eur. J.* **2003**, *9*, No. 1

mediate is the proposed final step leading to the hydroxylated cofactor and the oxo ferryl species Fe^{IV}=O (see Scheme 3). This species should be capable of inserting an oxygen atom into the C–H bond of phenyl rings.[18] As shown in the potential energy surface of Figure 5, the formation of the hydroxylating intermediate Fe^{IV}=O passes through two steps. The first involves elongation of the O–O bond toward an intermediate in which the O–O bond is not yet fully cleaved, while in the second 4a-carbinolamine is eventually formed. The same two-step mechanism for O–O cleavage was encountered in similar systems such as a non-heme biomimetic iron catalyst[44] and in cytochrome c oxidase.[45] The first transition state (Figure 7) occurs when the O–O distance is about 1.8 Å and requires a

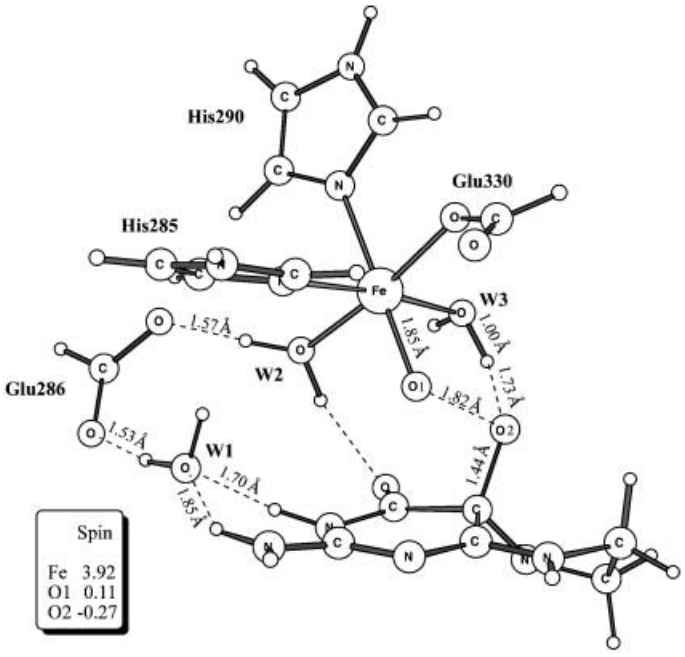

Figure 7. Optimized structure and spin distribution for the first transition state in O–O heterolysis.

barrier of 12.8 kcal mol^{-1} (relative to the initial iron dioxygen reactant). It then decays to a true minimum lying at 6.5 kcal mol^{-1} with an O–O distance of 2.16 Å; the geometry and the spin properties of this intermediate (denoted O–O intermediate in the following) are quite similar to those of the transition state (Table 2). During this first step of O–O heterolysis, the spin on iron increases and reaches 4.05 in the O–O intermediate. Simultaneously, some new spin appears on O2, the oxygen atom directly bound to C4a of pterin.

In the second step of the heterolytic cleavage the new O–H bond of the hydroxylated cofactor is formed. The water ligand W3, which forms a hydrogen bond to O2 of the iron dioxygen complex, is prepared to donate a hydrogen atom, as is also indicated by the very short hydrogen bond (1.59 Å) in the O–O intermediate. From this intermediate, the protonation of O2 occurs with hardly any barrier, since the related transition state (Figure 8) is calculated to lie at 6.5 kcal mol^{-1}, as shown in the potential energy surface of Figure 5. The calculated energy difference between this final transition state and the O–O intermediate is about 2 kcal mol^{-1}, but the solvent, entropy, and the zero-point effects cancel out any energy barrier.

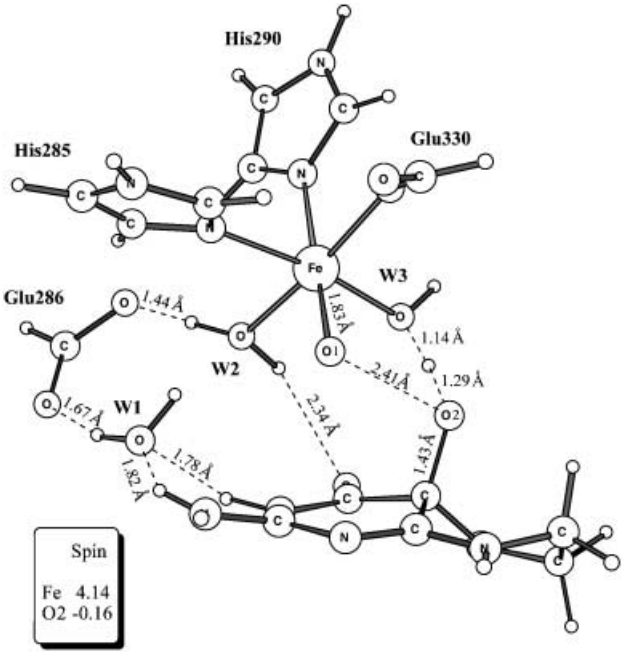

Figure 8. Optimized structure and spin distribution for the second transition state in O–O heterolysis.

A molecular orbital picture can provide a simple interpretation of the changes in the electronic distribution occurring during heterolytic O–O cleavage. In this picture, the coordination of the pterin-peroxide species at the metal center can be conveniently approximated as purely electrostatic, as suggested by the rather long Fe–O bond length of 2.07 Å (see Figure 6). To cleave the O–O bond, a β electron is initially promoted to the empty σ* O–O orbital, which implies that only one σ electron will effectively contribute to the O–O bond. The increase of total spin ($\alpha-\beta$) observed on the iron atom during the first step of the heterolytic process (Table 2) suggests that the β electron is supplied by the metal. The β electron in the antibonding O–O orbital, which leads effectively to half an O–O bond, explains the minimum occurring at a long O–O distance and it also accounts for the spin of -0.35 on O2 in the O–O intermediate. The lowest excited state of hydrogen peroxide, which has one β electron in the σ* O–O orbital, has a very similar minimum.[46] In the second step of O–O cleavage another electron, of α spin, must

Table 2. Geometric parameters [Å] and spin distributions for the transition state and the following O–O intermediate in the first step of O–O heterolysis.

	d(Fe–O1)	d(O1–O2)	d(O2–W3)	d(O2–C4a)	Spin(Fe)	Spin(O1)	Spin(O2)
transition state	1.85	1.82	1.73	1.44	3.92	0.11	−0.27
O–O intermediate	1.78	2.16	1.59	1.42	4.05	0	−0.35

  0947-6539/03/0901-0113 $ 20.00+.50/0

be promoted to the σ^* O–O orbital to cleave the O–O bond. This electron, which is again taken from the metal atom, is transferred during the formation of the new O–H bond. After O–O heterolysis and concomitant formation of the hydroxylated cofactor, the high-valent metal ion is generated, which forms the Fe=O double bond of the oxo ferryl species (Figure 9).

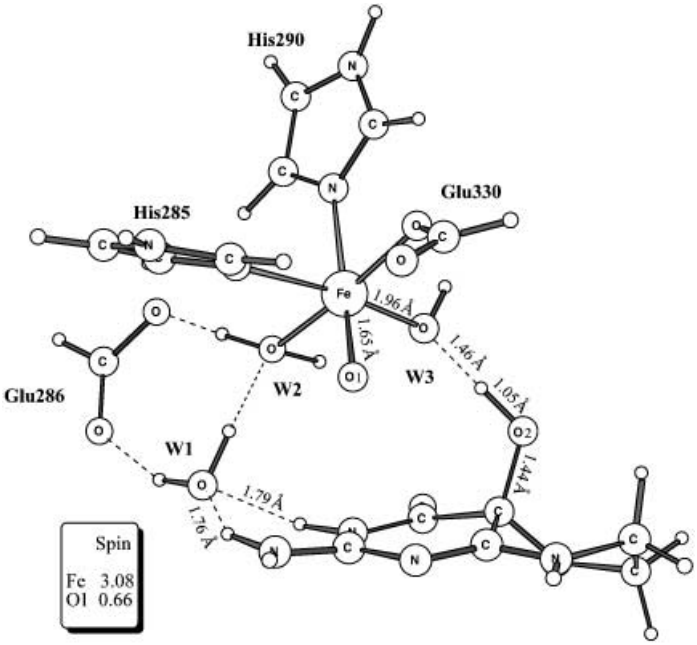

Figure 9. Optimized structure and spin distribution for the high-valent iron species Fe^{IV}=O, suggested to hydroxylate the aromatic amino acid.

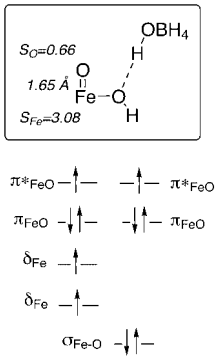

Figure 10. Qualitative molecular orbital picture describing the Fe^{IV}=O electronic structure.

The molecular orbital picture describing the Fe=O double bond[47] (Figure 10) accounts for the spin distribution on the iron atom. Two ferromagnetically coupled unpaired electrons occupy two degenerate π^* orbitals, and this results in localization of one electron on both the metal and the oxo group. Together with the original two unpaired electrons on the metal atom, a total spin of about three is then located on the iron center. The double bond, analogous to that in the O_2 molecule, also explains the short Fe–O bond length (1.65 Å).

As shown in Figure 5, the hydroxylation of the cofactor is driven by an exergonicity of 6.3 kcal mol^{-1}. It is noteworthy that the oxidized pterin is still protonated. The step which would lead to the unprotonated species could likely occur through the water molecules present at the active site,[21] but which are not included in the present model.

Conclusion

Based on the present DFT investigation, a mechanism for the first part of the catalytic cycle in aromatic amino acid hydroxylases is proposed (Figure 5), that is, formation of the hydroxylating intermediate.

Experiments[17] show that the Fe^{II} ion present in the active form of these enzymes is likely to be five-coordinate when the substrates bind, and it thus offers a free coordination site for dioxygen activation. The present studies indicate an essential role of iron at this stage of the reaction, since oxidation of the tetrahydrobiopterin cofactor can occur only if dioxygen enters the first coordination shell of iron and binds to the metal center. From the iron dioxygen complex the first step of oxygen reduction by the cofactor involves the formation of a new C4a–O bond to give to an iron(II)–peroxy–pterin intermediate. The analogous reduction of oxygen by the pterin cofactor, leading to a peroxy–pterin species without the involvement of the metal was found to be infeasible. In this step the presence of iron is thus essential for catalysis, and it is needed both to activate dioxygen and to stabilize the negative charge building up on the oxygen atom. No stable intermediate could be found in which pure electron transfer from the cofactor to dioxygen has occurred (i.e., a pterin carbocation radical and a superoxide ion O_2^-). The calculations further show that the rate-limiting step for the formation of the hydroxylating intermediate corresponds to C–O bond formation to give the iron(II)-peroxy-pterin intermediate. This intermediate then evolves by heterolytic O–O bond cleavage into C4a-hydroxypterin and the high-valent iron oxo species Fe^{IV}=O. The Fe^{IV}=O complex, referred to as the hydroxylating intermediate, is then ready to carry out hydroxylation of aromatic amino acids in the next part of the catalytic cycle.[18]

[1] T. J. Kappock, J. P. Caradonna, *Chem. Rev.* **1996**, *96*, 2659–2756.
[2] T. Flatmark, R. C. Stevens, *Chem. Rev.* **1999**, *99*, 2137–2160.
[3] P. Nordlund, in *Handbook of Metalloproteins* (Eds.: I. Bertini, A. Sigel, H. Sigel), Marcel Dekker, New York, **2001**, pp. 461–570.
[4] E. L. Hegg, L. Que, Jr., *Eur. J. Biochem.* **1997**, *250*, 625–629.
[5] L. Que, Jr., *Nature Struc. Biol.* **2000**, *7*, 182–184.
[6] G. Tian, J. P. Klinman, *J. Am. Chem. Soc.* **1993**, *115*, 8891–8897.
[7] W. A. Francisco, G. Tian, P. F. Fitzpatrick, J. P. Klinman, *J. Am. Chem. Soc.* **1998**, *120*, 4057–4062.
[8] P. F. Fitzpatrick, *Biochemistry* **1991**, *30*, 6386–6391.
[9] P. F. Fitzpatrick, *Biochemistry* **1991**, *30*, 3658–3662.
[10] J. P. Klinman, *J. Biol. Inorg. Chem.* **2001**, *6*, 1–13.
[11] H.-U. Siegmund, S. Kaufman, *J. Biol. Chem.*, **1991** *266*, 2903–2910.
[12] P. F. Fitzpatrick, *Annu. Rev. Biochem.* **1999**, *68*, 355–381.
[13] R. G. Moran, A. Derecskei-Kovacs, P. J. Hillas, P. F. Fitzpatrick, *J. Am. Chem. Soc.* **2000**, *122*, 4535–4541.
[14] T. A. Dix, G. E. Bollag, P. L. Domanico, S. J. Benkovic, *Biochemistry* **1985**, *24*, 2955–2958.
[15] M. Sono, M. P. Roach, E. D. Coulter, J. H. Dawson, *Chem. Rev.* **1996**, *96*, 2841–2887.
[16] T. D. H. Bugg, *Curr. Opin. Chem. Biol.* **2001**, *5*, 550–555.
[17] E. I. Solomon, T. C. Brunold, M. I. Davis, J. N. Kemsley, S.-K. Lee, N. Lehnert, F. Neese, A. J. Skulan, Y.-S. Yang, J. Zhou, *Chem. Rev.* **2000**, *100*, 235–349.
[18] S. J. Lange, H. Miyake, L. Que, Jr., *J. Am. Chem. Soc.* **1999**, *121*, 6330–6331.

0947-6539/03/0901-0114 $ 20.00+.50/0 *Chem. Eur. J.* **2003**, *9*, No. 1

[19] H. Erlandsen, E. Bjørgo, T. Flatmark, R. C. Stevens, *Biochemistry* **2000**, *39*, 2208–2217.
[20] K. E. Goodwill, C. Sabatier, R. C. Stevens, *Biochemistry* **1998**, *37*, 13437–13445.
[21] O. A. Andersen, T. Flatmark, E. Hough, *J. Mol. Biol.* **2001**, *314*, 279–291.
[22] P. W. Dickson, I. G. Jennings, R. G. H. Cotton, *J. Biol. Chem.* **1994**, *269*, 20369–20375.
[23] P. M. Nowacki, S. Byck, L. Prevost, C. R. Scriver, *Nucleic Acids Res.* **1998**, *26*, 220–225.
[24] K. Teigen, N. Å. Frøystein, A. Martinez, *J. Mol. Biol.* **1999**, *294*, 807–823.
[25] K. E. Loeb, T. E. Westre, T. J. Kappock, N. Mitić, E. Glasfeld, J. P. Caradonna, B. Hedman, K. O. Hodgson, E. I. Solomon, *J. Am. Chem. Soc.* **1997**, *119*, 1901–1915.
[26] J. N. Kemsley, N. Mitić, K. L. Zaleski, J. P. Caradonna, E. I. Solomon, *J. Am. Chem. Soc.* **1999**, *121*, 1528–1536.
[27] P. J. Stevens, F. J. Devlin, C. F. Chablowski, M. J. Frisch, *J. Phys. Chem.* **1994**, *98*, 11623–11627.
[28] A. D. J. Becke, *Chem. Phys.* **1993**, *98*, 5648–5652; **1992**, *96*, 2155–2160; **1992**, *97*, 9173–9177.
[29] C. Lee, W. Yang, R. G. Parr, *Phys. Rev.* **1988**, *B37*, 785–789.
[30] Jaguar 4.1, Schrödinger, Inc., Portland, Oregon, **2000**; See G. Vacek, J. K. Perry, J.-M. Langlois, *Chem. Phys. Lett.* **1999**, *310*, 189–194;
[31] Gaussian 98, M. J. Frisch, G. W. Trucks, H. B. Schlegel, G. E. Scuseria, M. A. Robb, J. R. Cheeseman, V. G. Zakrzewski, J. A. Montgomery, Jr., R. E. Stratmann, J. C. Burant, S. Dapprich, J. M. Millam, A. D. Daniels, K. N. Kudin, M. C. Strain, O. Farkas, J. Tomasi, V. Barone, M. Cossi, R. Cammi, B. Mennucci, C. Pomelli, C. Adamo, S. Clifford, J. Ochterski, G. A. Petersson, P. Y. Ayala, Q. Cui, K. Morokuma, D. K. Malick, A. D. Rabuck, K. Raghavachari, J. B. Foresman, J. Cioslowski, J. V. Ortiz, A. G. Baboul, B. B. Stefanov, G. Liu, A. Liashenko, P. Piskorz, I. Komaromi, R. Gomperts, R. L. Martin, D. J. Fox, T. Keith, M. A. Al-Laham, C. Y. Peng, A. Nanayakkara, C. Gonzalez, M. Challacombe, P. M. W. Gill, B. Johnson, W. Chen, M. W. Wong, J. L. Andres, C. Gonzalez, M. Head-Gordon, E. S. Replogle, and J. A. Pople, Gaussian, Inc., Pittsburgh, PA, **1998**.
[32] P. J. Hay, W. R. Wadt, *J. Chem. Phys.* **1985**, *82*, 299–310.
[33] D. J. Tannor, B. Marten, R. Murphy, R. A. Friesner, D. Sitkoff, A. Nicholls, M. Ringnalda, W. A. Goddard III, B. Honig, *J. Am. Chem. Soc.* **1994**, *116*, 11875–11882.
[34] B. Marten, K. Kim, C. Cortis, R. A. Friesner, R. B. Murphy, M. Ringnalda, D. Sitkoff, B. Honig, *J. Phys. Chem.* **1996**, *100*, 11775–11788.
[35] P. E. M. Siegbahn, *J. Comput. Chem.* **2001**, *22*, 1634–1645.
[36] P. E. M. Siegbahn, M. R. A. Blomberg, *Chem. Rev.* **2000**, *100*, 421–437.
[37] M. Wirstam, S. J. Lippard, R. A. Friesner, personal communication.
[38] L. A. Curtiss, K. Raghavachari, G. W. Tucks, J. A. Pople, *J. Chem. Phys.* **1991**, *94*, 7221–7230.
[39] L. A. Curtiss, K. Raghavachari, P. C. Redfern, J. A. Pople, *J. Chem. Phys.* **1997**, *106*, 1063–1079.
[40] N. Lehnert, R. Y. N. Ho, L. Que, Jr., E. I. Solomon, *J. Am. Chem. Soc.* **2001**, *123*, 8271–8290.
[41] Q. Su, J. P. Klinman, *Biochemistry* **1999**, *38*, 8572–8581.
[42] R. Prabhakar, P. E. M. Siegbahn, B. F. Minaev, H. Ågren, *J. Phys. Chem. B* **2002**, *106*, 3742–3750.
[43] M. A. Hill, J. J. A. Marota, R. Shiman, *J. Biol. Chem.* **1988**, *263*, 5646–5655.
[44] A. Bassan, M. R. A. Blomberg, P. E. M. Siegbahn, L. Que, Jr., *J. Am. Chem. Soc.* **2002**, *124*, 11056–11063.
[45] M. R. A. Blomberg, P. E. M. Siegbahn, M. Wikström, unpublished results.
[46] A. Bassan, M. R. A. Blomberg, P. E. M. Siegbahn, B. O. Roos, unpublished results.
[47] K. Yoshizawa, Y. Shiota, T. Yamabe, *J. Am. Chem. Soc.* **1998**, *120*, 564–572.

Received: April 29, 2002
Revised: September 9, 2002 [F4059]